10-1-1992

Seasonal and Latitudinal Variations of Gravity Wave-driven Fluctuations in OH Nightglow

Michael P. Hickey Ph.D.
Embry-Riddle Aeronautical University, hicke0b5@erau.edu

R. L. Walterscheid
The Aerospace Corporation

G. Schubert
Institute of Geophysics and Planetary Physics, University of California

Scholarly Commons Citation

Hickey, M. P., G. Schubert, and R. L. Walterscheid (1992), Seasonal and latitudinal variations of gravity wave-driven fluctuations in OH nightglow, J. Geophys. Res., 97(A10), 14911–14922, doi: https://doi.org/10.1029/92JA00795.

JOURNAL OF GEOPHYSICAL RESEARCH, VOL. 97, NO. A10, PAGES 14,911–14,922, OCTOBER 1, 1992

Seasonal and Latitudinal Variations of Gravity Wave-Driven Fluctuations in OH Nightglow

M. P. HICKEY[1]

FWG Associates, Huntsville, Alabama

G. SCHUBERT AND R. L. WALTERSCHEID

Space Science Laboratory, The Aerospace Corporation, Los Angeles, California

The seasonal and latitudinal variations of the gravity wave-driven fluctuations in the OH nightglow are investigated theoretically using a model that accounts for emission from an extended OH layer and includes the effects of eddy diffusivities in the gravity wave dynamics. The mean (unperturbed) state is obtained from a two-dimensional, nighttime model so that mean-state number densities, temperatures and eddy diffusivities are all self-consistent. Seasonal and latitudinal variations in the background OH nightglow emission and in the propagation and dissipation characteristics of the gravity waves influence how the OH nightglow modulations due to gravity waves depend on season and latitude. At intermediate gravity wave periods (i.e., periods between 0.5 and 3 hours for λ_x = 100 km; between 3 and 10 hours for λ_x = 500 km; and greater than about 4 hours for λ_x = 1000 km) possible trends in the behavior of $<\eta>$ (equal to $(<I'>/<\bar{I}>)/(<T_I'>/<\bar{T}_I>)$, where I is the airglow intensity, T is intensity-weighted temperature, an overbar denotes the mean state, a prime denotes a perturbation about that mean state and the brackets indicate vertical integration over all emission levels) with latitude and season could be masked by interference effects. At long periods (i.e., periods greater than 3 hours and 10 hours for λ_x = 100 and 500 km, respectively) trends are complicated by the competing effects of eddy diffusivities, which directly modify both local values of and the altitudes of maximum wave amplitude, and the vertical distributions of the minor species. Only at periods of a few hours or less (depending on horizontal wavelength) are any seasonal trends seen in $<\eta>$, and these are more noticeable in the magnitude of $<\eta>$ than in its phase. These seasonal variations in $<\eta>$ are primarily due to seasonal variations in the undisturbed temperature which affect the temperature-dependent chemical rate constants involved in the OH nightglow. A specific case showing latitudinal trends is presented, but the result is not representative of all of our results obtained involving latitudinal variations.

INTRODUCTION

The modulation of the intensity of the hydroxyl (OH) nightglow around the mesopause by the perturbing dynamical influences of internal gravity waves has been extensively modelled. The parameter η [*Krassovsky*, 1972], which relates the oscillation in the intensity I' about a mean intensity of the nightglow $\bar{I}$ to the oscillation in the temperature T' of the emission region about the mean temperature $\bar{T}$ by $\eta = (I'/\bar{I})/(T'/\bar{T})$, is a useful quantity calculated by these models because it can be determined experimentally and it is not dependent on the oscillation amplitude.

An initial model for such calculations by *Walterscheid et al.* [1987] used the Eulerian dynamics of linearized acoustic-gravity waves to upset the chemical equilibrium of the five minor species O, O_3, H, OH, and HO_2 controlling the concentration of excited OH. This thin layer model was also applied to the OH nightglow fluctuations induced by tides [*Walterscheid and Schubert*, 1987].

The modification of the model to account for the nonzero vertical extent of the emission region was performed by *Schubert and Walterscheid* [1988]. This modification was found to be important for waves having vertical wavelengths less than or comparable to the emission layer thickness because interference effects are important for these waves. This was also demonstrated by *Hines and Tarasick* [1987]. The thin layer model of *Walterscheid et al.* [1987] was also modified by *Hickey* [1988a, b] to include the effects of eddy momentum and thermal diffusivities in the gravity wave dynamics and was found to be important at long wave periods (or equivalently, at short vertical wavelengths). The fact that both interference effects and dissipation effects become important at short vertical wavelengths has led to their simultaneous inclusion in the most recent dynamical/chemical model of gravity wave-driven fluctuations in the OH nightglow [*Schubert et al.*, 1991]. In that study it was discovered that spurious results could be obtained if the upper boundary for the vertical integrations was not placed at a high enough altitude. Therefore the upper boundary was raised from its previous value of 95 km to 120 km, which is sufficiently high to ensure that all intensity-related perturbation variables approach zero there.

The values of $<\eta>$, $<I'/\bar{I}>$ and $<T'/\bar{T}>$ (the angle brackets indicate vertical integration over all emission levels) determined by these models depend on wave period, horizontal wavelength, atomic oxygen scale height, eddy Prandtl number, and eddy momentum diffusivity. These last three variables depend on the mean state of the mesosphere. To date, only one set of atmospheric parameters (those of *Winick* [1983]) has been used in the OH perturbation model. Further, the values of eddy diffusivity have so far been included in an ad hoc fashion

[1]Now at Physitron Incorporated, Huntsville, Alabama.

Paper number 92JA00795.
0148-0227/92/92JA-00795$05.00

(e.g., altitude independent) with no direct relation to the basic state atmospheric model. In this paper we remove this difficulty by using a more realistic basic state model atmosphere, the nightside mesosphere model of *Garcia and Solomon* [1985], in which several parameters vary together in a self-consistent way.

A weak seasonal variation in the OH emission has been predicted by *Le Texier et al.* [1987] using the two-dimensional dynamical-chemical model of *Garcia and Solomon* [1985] and has been verified experimentally [*Abreu and Yee,* 1989]. This variation is due to a seasonal variation in the vertical diffusion which in turn drives a seasonal variation in the atomic oxygen and atomic hydrogen densities. The seasonal variation in the vertical eddy diffusivity is due to a seasonal variation in gravity wave activity, which has an annual variation at high latitudes and a semiannual variation at low latitudes [*Hirota,* 1984; *Garcia and Solomon,* 1985]. Thus the seasonal and latitudinal variations of eddy diffusivities will affect the gravity wave-driven fluctuations in an extended OH nightglow layer by affecting both the chemistry and the altitude variation of the amplitudes of the driving gravity waves. Whether or not a seasonal or latitudinal variation is reflected in the derived OH nightglow modulations due to gravity waves will depend on the altitude integration of a complex convolution between gravity wave phase and amplitude and OH nightglow chemistry.

The purpose of the present paper is to use a self-consistent atmospheric model as an input to the OH fluctuation model in order to examine if there are any seasonal and latitudinal variations in the characteristics of the derived OH nightglow fluctuations. We focus on the vertically integrated Krassovsky's ratio $<\eta>$ because there is a general lack of information on latitudinal and seasonal variations of wave amplitudes and $<\eta>$ is the only modelled parameter that is independent of wave amplitude.

THEORY

The OH fluctuation model has been described before, and details can be found in the works by *Schubert et al.* [1991], *Hickey* [1988a], *Schubert and Walterscheid* [1988] and *Walterscheid et al.* [1987]. Here the effects of eddy viscosity and eddy thermal diffusivity are modelled as analogous to that of molecular viscosity and molecular thermal diffusivity by employing the acoustic-gravity wave formulas of *Hickey and Cole* [1987]. The more general approach of *Schubert et al.* [1991] gives essentially the same results but is more computationally intensive.

Output from the model atmosphere of *Garcia and Solomon* [1985] is used to determine the number densities of the major gas (N_2 and O_2) and the minor species OH, H, O_3, O and HO_2, the temperature, and the eddy momentum diffusivity. This model output, provided by Rolando Garcia (private communication, 1990) and Helene Le Texier (private communication, 1989) only extends to a little over 100 km altitude. Therefore the various model outputs were extrapolated to 120 km altitude by assuming constant scale heights at and above 100 km (in the case of species number densities) and constant gradients at and above 105 km altitude (in the case of temperature and eddy diffusivity). The *Garcia and Solomon* [1985] numerical model of the dynamical and chemical structure of the nightside middle atmosphere includes *Lindzen's* [1981] parameterization of breaking gravity waves, *Lindzen and Forbes'* [1983] parameterization of nonbreaking gravity waves, and *Lindzen's* [1981] parameterization of the breaking gravest vertically propagating diurnal tidal mode. For consistency with *Garcia and Solomon* [1985], the Prandtl number is taken equal to 2 in the calculation of the thermal diffusivity.

Reactions between H and O_3 and between O and HO_2 are assumed to be responsible for the OH nightglow, such that OH* is produced in a single vibrationally excited state. Because the effects of quenching are not considered here, the background intensity $\bar{I}$ of excited OH* does not have a well-defined peak for June at 82°N, but instead shows a local minimum. In this case a single exponential factor multiplied $\bar{I}$ to decrease it to $\exp(-6)\,\bar{I}_{peak}$ at the lower boundary. Sensitivity studies involving reduction of the artificial quenching so that $\bar{I}$ was only $\exp(-2.3)\,\bar{I}_{peak}$ (about $0.1\,\bar{I}_{peak}$) at the lower boundary have shown that the overall results are not seriously affected by this procedure. (This "artificial quenching" was in fact accomplished by multiplying the rate constants by the above factors, thereby ensuring that the gravity wave intensity perturbations were similarly "quenched.")

The lower boundary of the model is at 75 km and the upper boundary is at 120 km. The gravity waves at the lower boundary have a relative temperature amplitude set equal to unity, independent of latitude and season. As previously explained, this will not impact the results presented here because $<\eta>$ is independent of wave amplitude.

RESULTS

Background States

Relevant characteristics of the undisturbed nightside mesosphere, as obtained from the model of *Garcia and Solomon* [1985], are shown in Figures 1 through 4. Figure 1 shows the momentum diffusivity K_{zz} as a function of altitude for different seasons (March, June, September, and December) and latitudes (82°N, 68°N, 39°N, and 18°N). Figures 2 and 4 are similar presentations of temperature and hydroxyl nightglow intensity. Figure 3 shows altitude profiles of minor constituent number density for December and for latitudes of 18°N and 82°N.

The eddy momentum diffusivity K_{zz} (Figure 1) is relatively constant with altitude between about 75 and 100 km (see, for example, the altitude profiles of K_{zz} for December) although there is a tendency for K_{zz} to increase somewhat with height and even undergo nonmonotonic variations with altitude (see in particular the altitude profiles of K_{zz} for June). In the 75- to 100-km altitude range, K_{zz} generally has values varying between about 50 and 200 $m^2\ s^{-1}$. Eddy momentum diffusivity generally increases dramatically with height between about 100 and 120 km, especially during the solstices and at high latitudes during the equinoxes, reaching values of about $10^3\ m^2\ s^{-1}$ at 120 km. During the equinoxes and at low latitudes, K_{zz} increases more gradually and uniformly with height over the entire altitude range 75 to 120 km, attaining values at 120 km between about 500 and 800 $m^2\ s^{-1}$ (March, 18°N is an exception).

The extrapolation of model predictions of K_{zz} above 105 km altitude leads to unrealistically large values of K_{zz} at these altitudes. However, the effects of dissipation on the gravity waves due to the large values of molecular kinematic viscosity that actually exist above 105 km altitude are approximated

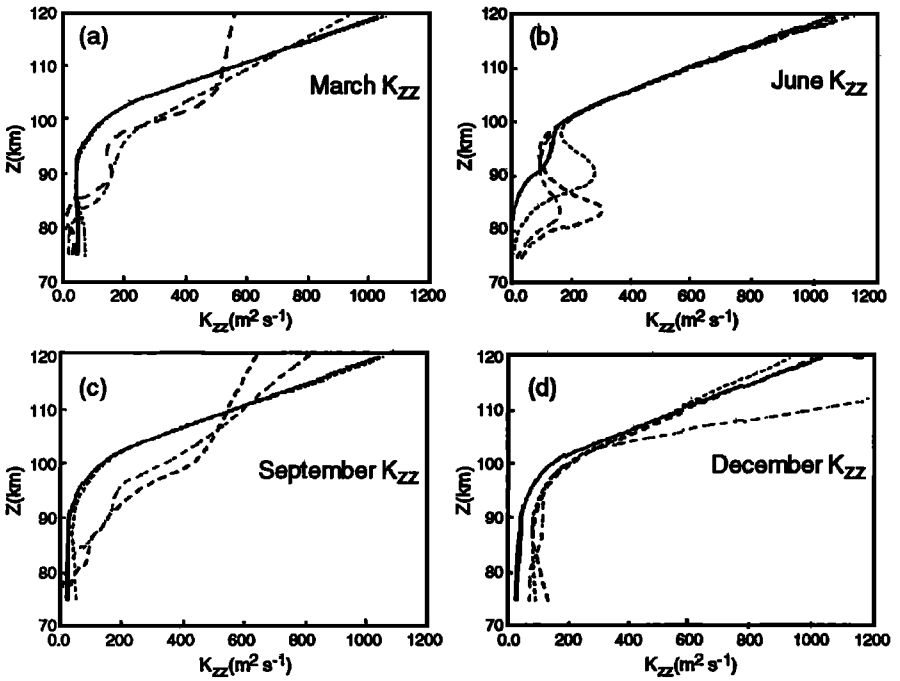

Fig. 1. Eddy momentum diffusivity (K_{zz}) as a function of altitude for each season and for latitudes of 82°N (solid curve), 68°N (short-dashed curve), 39°N (long-dashed curve) and 18°N (dot-dashed curve) obtained from the model of *Garcia and Solomon* [1985].

quite well by the extrapolated K_{zz} values used in this paper. Our results and conclusions are not sensitive to the specific values of K_{zz} near the upper boundary of the model. The values of K_{zz} employed strongly attenuate the long-period gravity waves before they reach the upper boundary of the model in order to alleviate the spurious interference effects discussed by *Schubert et al.* [1991]. This would also occur had we included molecular dissipation in the model.

The latitudinal and seasonal variations of temperature are displayed in Figure 2. The mesopause region is especially broad (in altitude) and nearly isothermal in September with temperatures around 190 K over altitudes between about 80 and

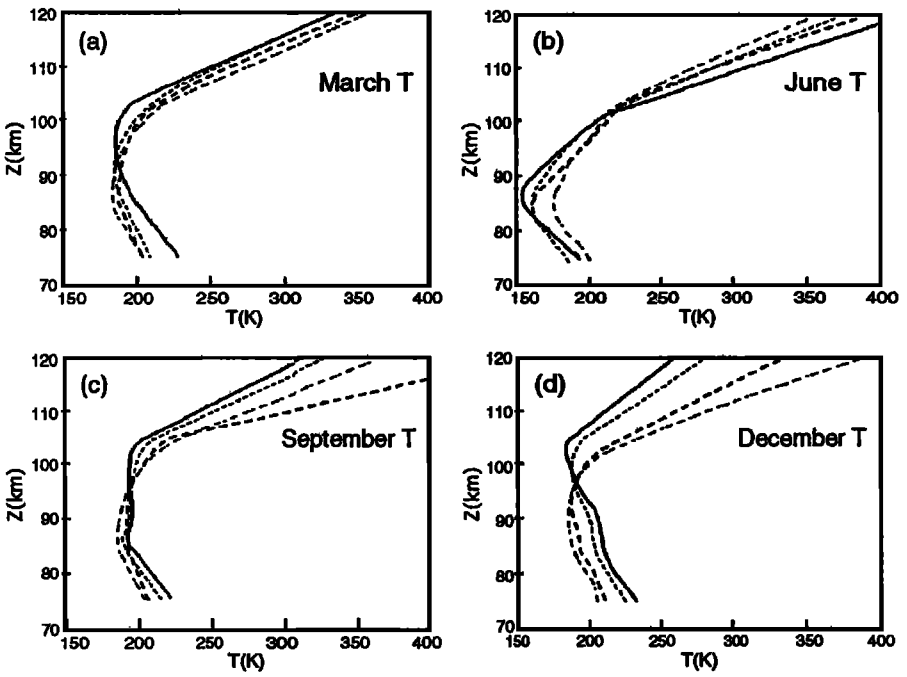

Fig. 2. Temperature as a function of altitude for each season and for latitudes of 82°N (solid curve), 68°N (short-dashed curve), 39° (long-dashed curve) and 18°N (dot-dashed curve) obtained from the model of *Garcia and Solomon* [1985].

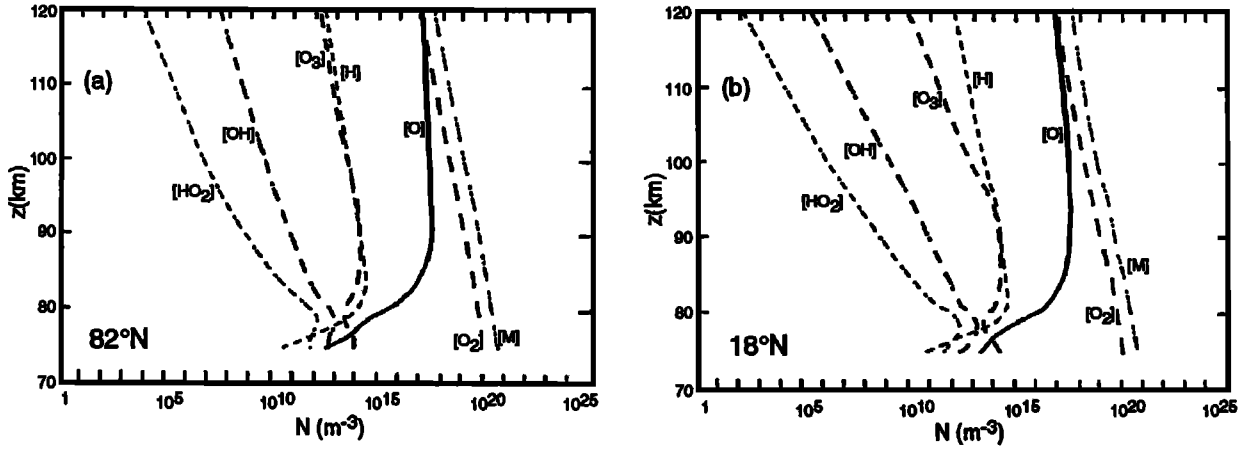

Fig. 3. Species number densities as a function of altitude for December and for latitudes of (a) 82°N and (b) 18°N, obtained from the model of *Garcia and Solomon* [1985].

100 km. The mesopause is also relatively broad and almost isothermal in March, except for the northernmost latitude of 82°N. The temperatures and heights of the mesopause region are broadly similar for March and September; the main difference between the March and September mesopause regions is the somewhat higher vertical extent (by 5 to 10 km) of the September mesopause. The June mesopause is colder (by as much as nearly 50 K) and at a lower altitude (by as much as nearly 20 km) than the December mesopause. During the solstices the mesopause height generally increases with increasing latitude; this trend is also characteristic of the equinoxes though the broad, approximately isothermal nature of the equinox mesopause partly masks the trend. Mesopause temperature decreases with increasing latitude in June, but is roughly constant with latitude at other times of the year. The differences between mesopause temperatures in June and December increase as latitude increases. Above about 100 km temperature decreases with increasing latitude except for June

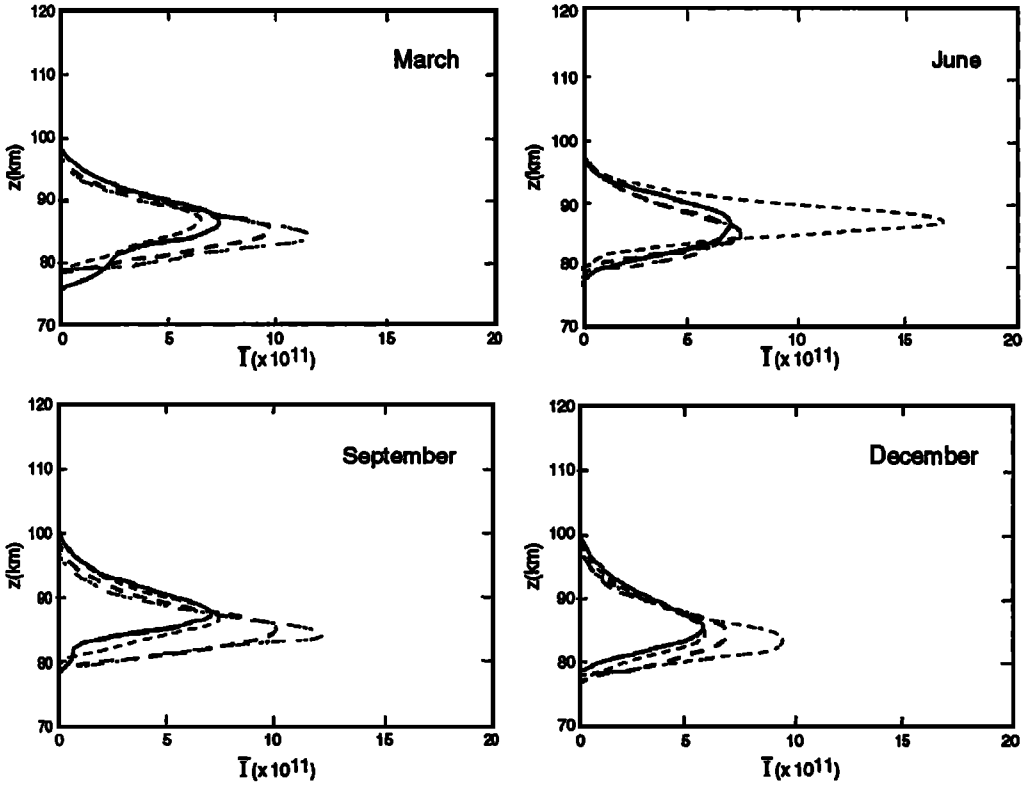

Fig. 4. The undisturbed OH nightglow emission as a function of altitude for each season and for latitudes of 82°N (solid curve), 68°N (short-dashed curve), 39°N (long-dashed curve) and 18°N (dot-dashed curve) obtained from the model of *Garcia and Solomon* [1985]. The emission intensity was calculated by assuming that all excited OH radiates and that both the ozone and the perhydroxyl reactions contribute to the emission. See text for details.

when the trend is essentially reversed (September, 39°N is another exception). Below about 100 km temperature increases with increasing latitude, except for an approximate reversal of the trend in June and at low altitudes for September, 39°N.

Altitude profiles of the number densities of the minor species H, O, HO_2, O_3 and OH and the major gas ($M=O_2+N_2$) are shown in Figures 3a and 3b for latitudes of 82°N and 18°N, respectively, and for the month of December. Below about 80 km, the atomic oxygen and hydrogen densities at 82°N are considerably smaller than those at 18°N due to a lack of solar photodissociation in the high latitude winter mesosphere. (The model output of Garcia and Solomon actually produced values of zero for the O and H densities below about 80 km altitude for wintertime 82°N but here these densities have been set to very small, nonzero values in order to avoid any discontinuity problems with our curve fitting routines. The smallness of these densities does not affect the results or conclusions of this paper.) At higher altitudes O and H densities are similar for the two latitudes. At altitudes around 80 km, O_3 densities are similar for the two latitudes, but at greater altitudes these densities are significantly greater at 82°N (by a factor of about 300 at 120 km) than at 18°N. This is due to the increase in ozone-destroying solar radiation at the lower wintertime latitudes. Hydroxyl densities at 82°N are greater than those at 18°N above about 85 km altitude, with the ratio of OH density between the polar and equatorial latitudes being about 100 at 120 km. Below this altitude the OH densities are comparable at the two latitudes. Between about 83 and 92 km altitude HO_2 densities are similar for both latitudes; outside of this altitude range these densities are greater at 82°N than at 18°N.

Figure 4 shows altitude profiles of the undisturbed OH* emission $\bar{I}$ for the different seasons and latitudes. As described in the theory section, artificial quenching has been applied for June at 82°N. The emission profiles for March are similar to those of September, with the major difference being that $\bar{I}$ is slightly larger at 82°N than at 68°N in March while the reverse is true in September. For March and September $\bar{I}$ peaks at an altitude some 2 km higher at high latitudes than it does at the lower latitudes. For both of these months the low-latitude peak values of $\bar{I}$ are larger than those at high latitudes. The December set of emission profiles is most similar to the September set, with the major differences being a 1- or 2-km drop in the altitudes of the emission peaks in December with corresponding decreases (by as much as 30%) in the peak intensities. The largest peak intensity of any emission profile occurs in June at 68°N. The June emission profiles at 18°N and 39°N are similar to each other, both peaking at an altitude of about 84 km. The June 82°N emission profile peaks at an altitude of about 86 km with a peak intensity slightly smaller than the low-latitude peak intensities.

Nightglow Fluctuations

Latitudinal variations. We illustrate the latitudinal variations occurring in OH nightglow fluctuations by considering the month of September and a horizontal disturbance wavelength of 500 km. Because $<\eta>$ is determined in part by wave dynamics, we first discuss the latitude variations in the real and imaginary parts of the complex wavenumber k_z.

The vertical wavelength λ_z ($\lambda_z = 2\pi\{\text{Real}(k_z)\}^{-1}$) of the gravity wave, an important wave parameter in this model

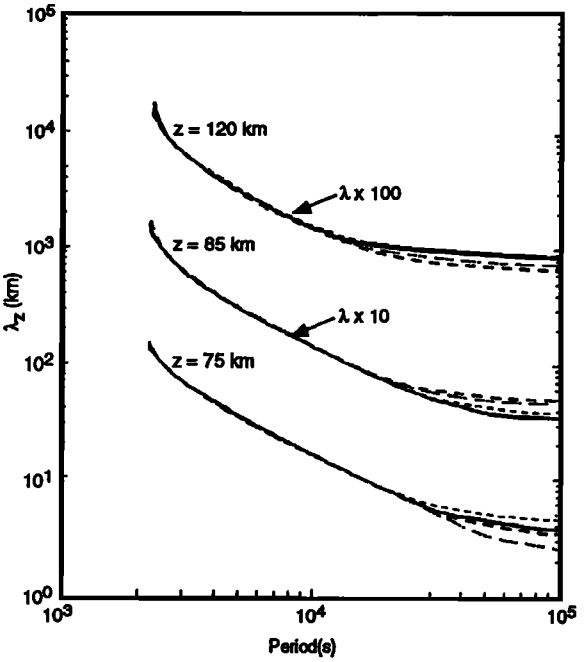

Fig. 5. Vertical wavelength for September and for λ_x = 500 km and for latitudes of 82°N (solid curve), 68°N (short-dashed curve), 39°N (long-dashed curve) and 18°N (dot-dashed curve) at altitudes of 75, 85 and 120 km as a function of wave period. Note that the curves for z = 85 and 120 km altitude have been multiplied by factors of 10 and 100, respectively.

[*Schubert et al.*, 1991], is plotted as a function of wave period for each latitude and for altitudes of 75, 85 and 120 km in Figure 5. At short periods ($< 10^4$ s) λ_z is similar at all altitudes and latitudes due to the smallness of dissipation at short periods. At long periods, where the effects of dissipation become important, λ_z is latitude dependent because K_{zz} depends on latitude. The effect of dissipation is to increase vertical wavelengths, so that λ_z asymptotes to a constant value at long periods [*Hickey*, 1988a, b; *Schubert et al.*, 1991; M. P. Hickey, a dispersion equation for long-period gravity waves in the mesosphere, submitted to *Journal of Geophysical Research*, 1991]. At long periods λ_z increases between 75 and 85 km by an increasing amount during progression from high to low latitudes. At 75 and 120 km altitude and at long periods the high latitude values of λ_z are greater than those at low latitudes, while at 85 km the reverse is true. Between 85 and 120 km altitude at long periods all values of λ_z increase, especially the high-latitude values.

The imaginary part of k_z ($Im(k_z)$) is shown as a function of period in Figure 6 in a format similar to that of λ_z in Figure 5. Note that although the standard 1/2H term is not included in the values of the imaginary part of k_z shown in Figure 6, it has nonetheless been included in all of our computations. At the shorter wave periods (period < 4×10^4 s) where dissipation is moderate, $|Im(k_z)|$ increases between 75 and 85 km altitude at all latitudes except 68°N. At 120 km altitude dissipation becomes important at shorter periods than it does at lower altitudes due to the larger values of K_{zz} there. When the dissipation is moderate, $|Im(k_z)|$ is larger at 120 km than at the lower altitudes for all latitudes. However, at longer periods where dissipation is more important, $|Im(k_z)|$ is largest at the

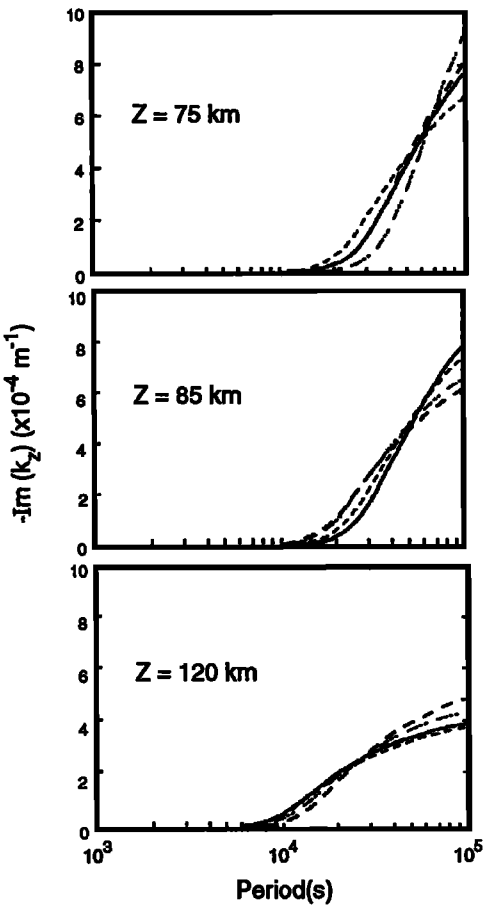

Fig. 6. Imaginary k_z for September and for λ_x = 500 km and for latitudes of 82°N (solid curve), 68°N (short-dashed curve), 39°N (long-dashed curve) and 18°N (dot-dashed curve) at altitudes of 75, 85 and 120 km as a function of wave period.

lowest altitude where K_{zz} is smallest. This surprising behavior is due to the complex coupling that occurs between $Re(k_z)$ and $Im(k_z)$ whenever dissipation is significant. When dissipation is small the coupling is absent [*Pitteway and Hines*, 1963] and $|Im(k_z)| \propto K_{zz}$, but when the dissipation is significant $|Im(k_z)| \propto K_{zz}^{-1/3}$ (M. P. Hickey, submitted paper). Effects of such coupling, when dissipation is important, have also been discussed by *Klostermeyer* [1972] and *Hickey and Cole* [1988]. Dissipation is larger for smaller vertical wavelengths, and as shown in Figure 5, at long periods (period > $6x10^4$ s) λ_z is smaller at 75 km than at 120 km altitude. At 120 km the variation in $Im(k_z)$ with latitude is at most about 25%.

The magnitude of $<\eta>$ (= $(<I'>/<\bar{I}>)/(<T_{I'}>/<\bar{T}_I>)$) is shown as a function of wave period for each latitude in Figure 7a, while its phase is shown in Figure 7b. Strong interference peaks and troughs are evident in $|<\eta>|$ for 18°N and 68°N. For 39°N and for periods greater than about $2x10^4$ s $|<\eta>|$ remains constant with a value of about 23. At short periods (period < 10^4 s) all values of $|<\eta>|$ are similar. At periods of about 10^4 s the values of $|<\eta>|$ fall into either a high (82°N and 68°N) or a low (18°N and 39°N) latitude group, with the high-latitude values of $|<\eta>|$ exceeding those of the low-latitude group. As the period is increased beyond 10^4 s these trends quickly disappear as the effects of interference become dominant. At intermediate periods (periods between about 10^4 s and $5x10^4$ s) possible trends could be masked by interference effects. At long periods (periods > $5x10^4$ s) there is considerable spread in the values of $|<\eta>|$, with the high-latitude $|<\eta>|$ values being smaller than their low-latitude counterparts. Long-period values of $|<\eta>|$ at 82°N are typically about 10. There is a general trend for $|<\eta>|$ to decrease with increasing latitude at long periods (periods > $5x10^4$ s) and to increase with increasing latitude at short periods (periods < 10^4 s). This trend is weak, however, because the values of $|<\eta>|$ for 18°N and 39°N would need to be interchanged for the trend to hold.

At short periods the phase of $<\eta>$ (Figure 7b) falls into either a high (82°N and 68°N) or a low (18°N and 39°N) latitude group. This trend becomes more noticeable as periods increase to about 10^4 s, after which a further increase in period causes the effects of interference to dominate and mask any latitudinal trends. At long periods there are no obvious latitudinal trends in the phase of $<\eta>$.

Some latitudinal trends in our derived values of $<\eta>$ were noted for other seasons. In March and for λ_x = 100 km, $|<\eta>|$ increases with increasing latitude for periods less than about 0.5 hour, but the total increase is by less than 5 percent. In March and for λ_x = 500 km, values of $|<\eta>|$ fall into either a low- or a high-latitude group for periods between about 1 and 4 hours with the low-latitude values of $|<\eta>|$ exceeding the high-latitude values (at a period of about 2 hours, $|<\eta>|$ is about 5 for the high-latitude group and about twice that for the low-latitude group). Finally, in June and for λ_x = 1000 km, values of $|<\eta>|$ fall into either a low- or a high-latitude group for periods between about 2 and 5 hours, with the low-latitude values of $|<\eta>|$ exceeding the high-latitude values (at periods close to 4 hours, $|<\eta>|$ is about 4.5 for the high-latitude group and about twice that for the low-latitude group). Generally, there were less noticeable trends in our derived phases of $<\eta>$, and relative changes associated with these phases were always much smaller than those associated with the magnitude of $<\eta>$. Systematic latitudinal trends for each combination of season and λ_x were, in general, not found. The results described above which include the September, λ_x = 500 km results, constitute all of our results displaying any significant latitudinal trends.

Seasonal variations. We next examine the seasonal variations of gravity wave-driven fluctuations in the OH nightglow at a fixed latitude. Examination of our results reveals that there are seasonal variations in $|<\eta>|$ only at wave periods of a few hours or less (the exact values depending on the value of horizontal wavelength). Therefore only values of $|<\eta>|$ for these periods will be presented. All subsequent figures illustrating seasonal variations will be comprised of four sets of plots, each plot displaying $|<\eta>|$ as a function of period for all seasons at a particular latitude. Seasonal variations at intermediate and long periods could be masked by the effects of interference.

Figure 8a shows $|<\eta>|$ displayed for λ_x = 100 km. The wave periods range from 500 s to 10^3 s (8.3 min to 16.7 min). Clearly, $|<\eta>|$ is largest in June and smallest in December. The values of $|<\eta>|$ for the equinoxes lie in between the solstice values, with the values of $|<\eta>|$ for March generally exceeding those of September. While there is a comparatively large separation in the values of $|<\eta>|$ between June and December at all latitudes, there is very little difference between values of $|<\eta>|$ for March and September.

The phase of $<\eta>$ for λ_x = 100 km (Figure 8b) is smallest (most negative) in June at low latitudes (18°N and 39°N) and smallest in September at high latitudes (82°N and 68°N). At low latitudes the phase of $<\eta>$ is largest (most positive) in

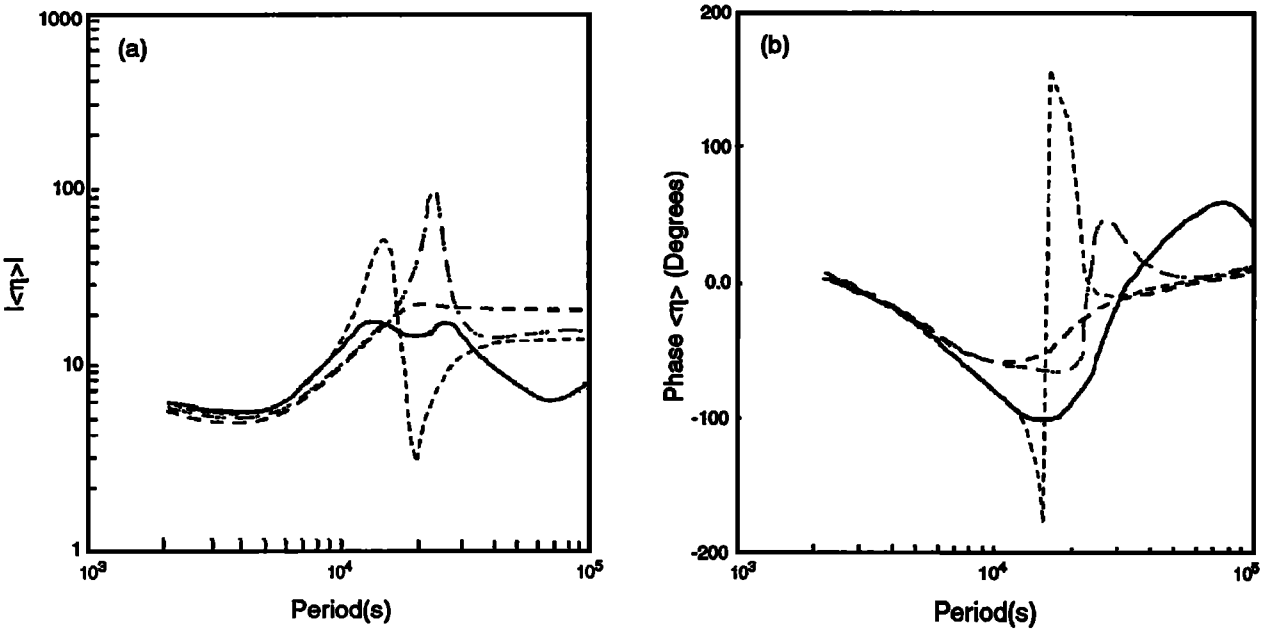

Fig. 7. (a) Magnitude and (b) phase of $<\eta>$ as a function of wave period for September and for λ_x = 500 km and for latitudes of 82°N (solid curve), 68°N (short-dashed curve), 39°N (long-dashed curve) and 18°N (dot-dashed curve).

December, with the phase values of the equinoxes being similar to each other and lying between those of June and December. At 68°N latitude and for periods greater than about 10 min the phase of $<\eta>$ is largest in December with the phase values of March and June lying between those of September and December. At 82°N the phase of $<\eta>$ is smallest in September and largest in March, with the phase values of the solstices being similar to each other and lying between those of the equinoxes. The trends that were observed in our results for $|<\eta>|$ are not the same as those found in the phase of $<\eta>$.

Figure 9a shows the seasonal plots of $|<\eta>|$ for λ_x = 500 km. The wave periods range from 2000 s to 10^4 s (33 min to 2.8 hours). For the latitudes of 18°N and 39°N, $|<\eta>|$ is largest for the month of June at all periods. For periods less than about 5000 s (1.4 hours) $|<\eta>|$ is smallest in December at all latitudes. At the shortest periods (< 4000 s) the values of $|<\eta>|$ for March and September are bounded above and below by the $|<\eta>|$ values for June and December, respectively, at all latitudes. At the lowest latitudes this relationship holds for periods up to 6000 s (18°N) and 5000 s (39°N). September $|<\eta>|$ values generally exceed those for December at all latitudes (with one minor exception at 39°N). The September values of $|<\eta>|$ exceed the March values for periods at the high end of the period range considered at all latitudes, contrary to the results for the λ_x = 100 km case. At all latitudes March values of $|<\eta>|$ exceed those of December at the low end of the period range with the opposite generally true at the high end of the period range.

The phase of $<\eta>$ for λ_x = 500 km (Figure 9b) is smallest in June at low latitudes (18°N and 39°N) and smallest in September at high latitudes (82°N and 68°N), as was the case for λ_x = 100 km. At low latitudes and for periods less than about 8000 s the phase of $<\eta>$ is largest in March, while the September and December phase values are similar to each other. At 68°N and for periods less than about 9000 s the phase of $<\eta>$ is largest in June. At 82°N the phase of $<\eta>$ is largest in either March or June, depending on the value of wave period. The oscillatory behavior in the phase of $<\eta>$ for June at 82°N is due to the dominance of the effects of interference, which causes a rapid increase in the phase of $<\eta>$ at periods close to 10^4 s. For periods less than about 7500 s and at 82°N the phase of $<\eta>$ in December is similar to, but slightly greater than that of September. Trends that we see in the seasonal variations of $|<\eta>|$ are not reflected in the seasonal variations in the phase of $<\eta>$.

Figure 10a shows the seasonal plots of $|<\eta>|$ for λ_x = 1000 km. The wave periods range from 4000 s to 10^4 s (1.1 hours to 2.8 hours). At 18°N and 39°N $|<\eta>|$ is largest in June. At 18°N, $|<\eta>|$ is essentially smallest in December for all periods less than 10^4 s (2.8 hours). At 18°N the values of $|<\eta>|$ for the equinoxes lie between those of the solstices. At all latitudes the September $|<\eta>|$ values exceed those of March and December for the range of periods considered (this is contrary to the λ_x = 100 km case where March values of $|<\eta>|$ exceeded those of September). At high latitudes the seasonal behavior in $|<\eta>|$ is quite different from that at lower latitudes or from the previous results shown for the other wavelengths, with no obvious trends.

The phase of $<\eta>$ for λ_x = 1000 km (Figure 10b) is largest in March at low latitudes and largest in June at high latitudes. At low latitudes the phase values of $<\eta>$ are similar to each other in June, September and December. At 68°N the phase of $<\eta>$ decreases as we progress from June to March to December to September. This is similar to the phase behavior we observe in our results at 82°N, except that for periods less than about 7000 s the phase of $<\eta>$ for December slightly exceeds that of September. Once again, any trends that we see in the seasonal variations of $|<\eta>|$ are not reflected in the seasonal variations of the phase of $<\eta>$.

SUMMARY OF RESULTS

The effects of interference change rapidly with wave period and are most noticeable in our results at intermediate gravity

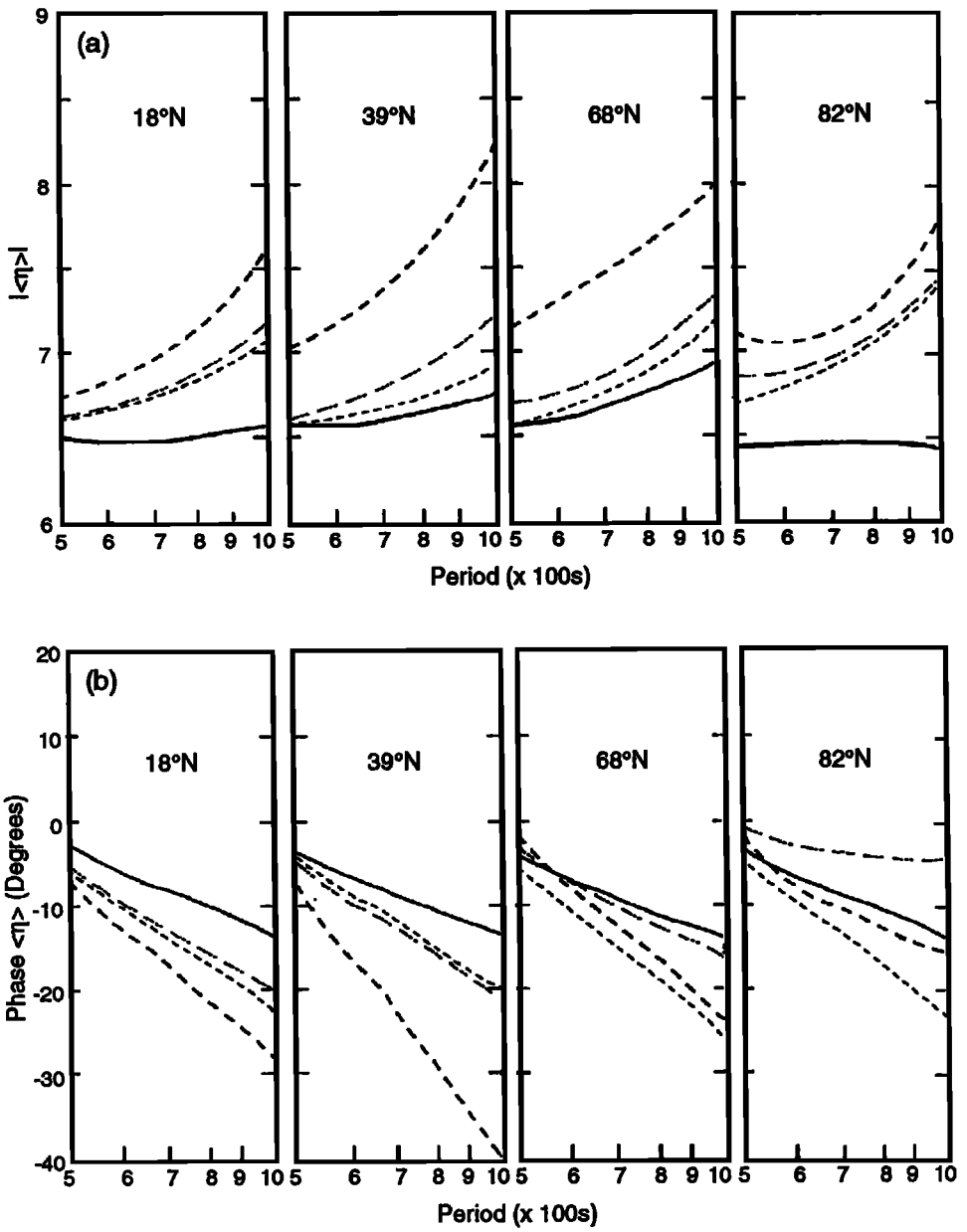

Fig. 8. (a) Magnitude and (b) phase of $<\eta>$ as a function of wave period for $\lambda_x = 100$ km for March (dot-dashed curve), June (long-dashed curve), September (short-dashed curve) and December (solid curve) for each latitude.

wave periods, i.e., periods long compared to evanescent wave periods and shorter than the longest periods chosen for this study (10^5 s). At these intermediate periods, any possible trends, either of a seasonal or a latitudinal nature, are complicated and could consequently be masked by the interference effects.

At long wave periods, the effects of dissipation become severe. These waves attain their maximum amplitudes in the lower altitude regions of the model, and thus the calculated nightglow fluctuation characteristics are determined by the prevailing atmospheric (chemical) state at these lower altitudes. However, these characteristics also depend directly on the effects of the eddy diffusivities themselves [*Hickey*, 1988a, b; *Schubert et al.*, 1991]. This complicated convolution tends to wipe out any seasonal or latitudinal trends at long periods, primarily because changes in the fluctuation characteristics due to changes in chemistry may be mitigated or even totally overshadowed by the changes in the fluctuation characteristics due to changes in K_{zz}.

At short wave periods the effects of dissipation are at most minimal. These waves attain their maximum amplitudes in the higher altitude regions of the model, and thus the calculated nightglow characteristics are determined primarily by the prevailing chemical state at altitudes around the peak of the undisturbed OH nightglow intensity. Thus any seasonal or latitudinal variation in the background state should result in a corresponding variation in the OH nightglow modulation characteristics, independent of the values of eddy diffusivities.

For the first case considered, that of a wave with a 500-km horizontal wavelength for the month of September, we found that both the magnitude and the phase of $<\eta>$ could be grouped according to low or high latitude for a limited range of periods

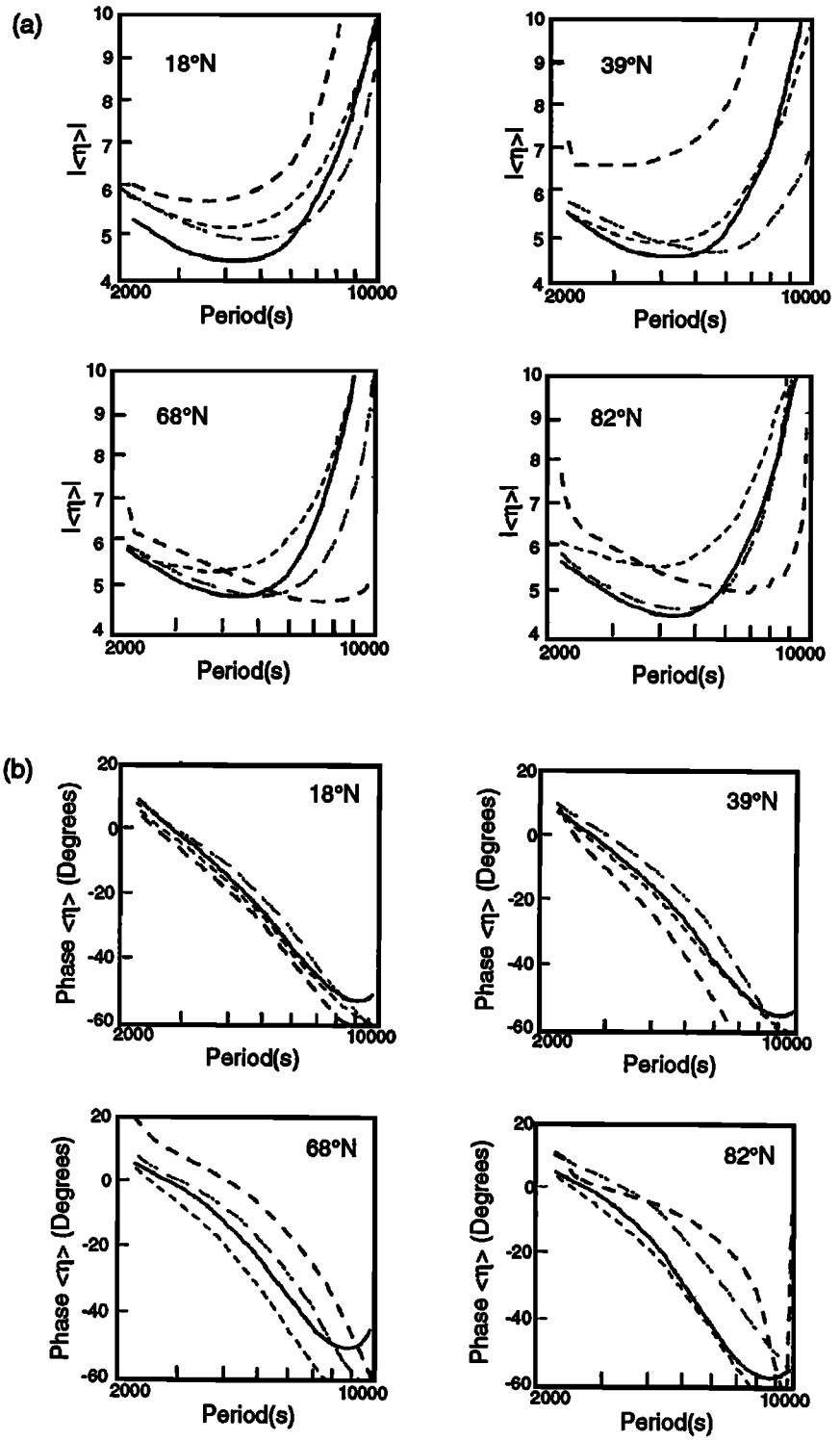

Fig. 9. Similar to Fig. 8 except that λ_x = 500 km.

located around 10^4 s. Other trends were noted in the magnitude of $<\eta>$ for periods ranging from 0.5 hour up to about 5 hours for three other combinations of λ_x and season, but overall for the 12 remaining combinations of λ_x and season there were no systematic latitudinal trends.

We also examined the seasonal variations in the OH nightglow fluctuation characteristics for each combination of latitude and wavelength. The clearest trends were seen in the results for λ_x = 100 km, where at short periods $|<\eta>|$ was largest in June and smallest in December, with the two equinox values of $|<\eta>|$ being similar to each other. However, for this same wavelength, clear trends in the phase of $<\eta>$ were only seen at low latitudes. At low latitudes and at short periods $|<\eta>|$ was consistently largest in June for all of the wavelengths considered. Except for the λ_x = 1000 km case, $|<\eta>|$ was smallest in December at all latitudes.

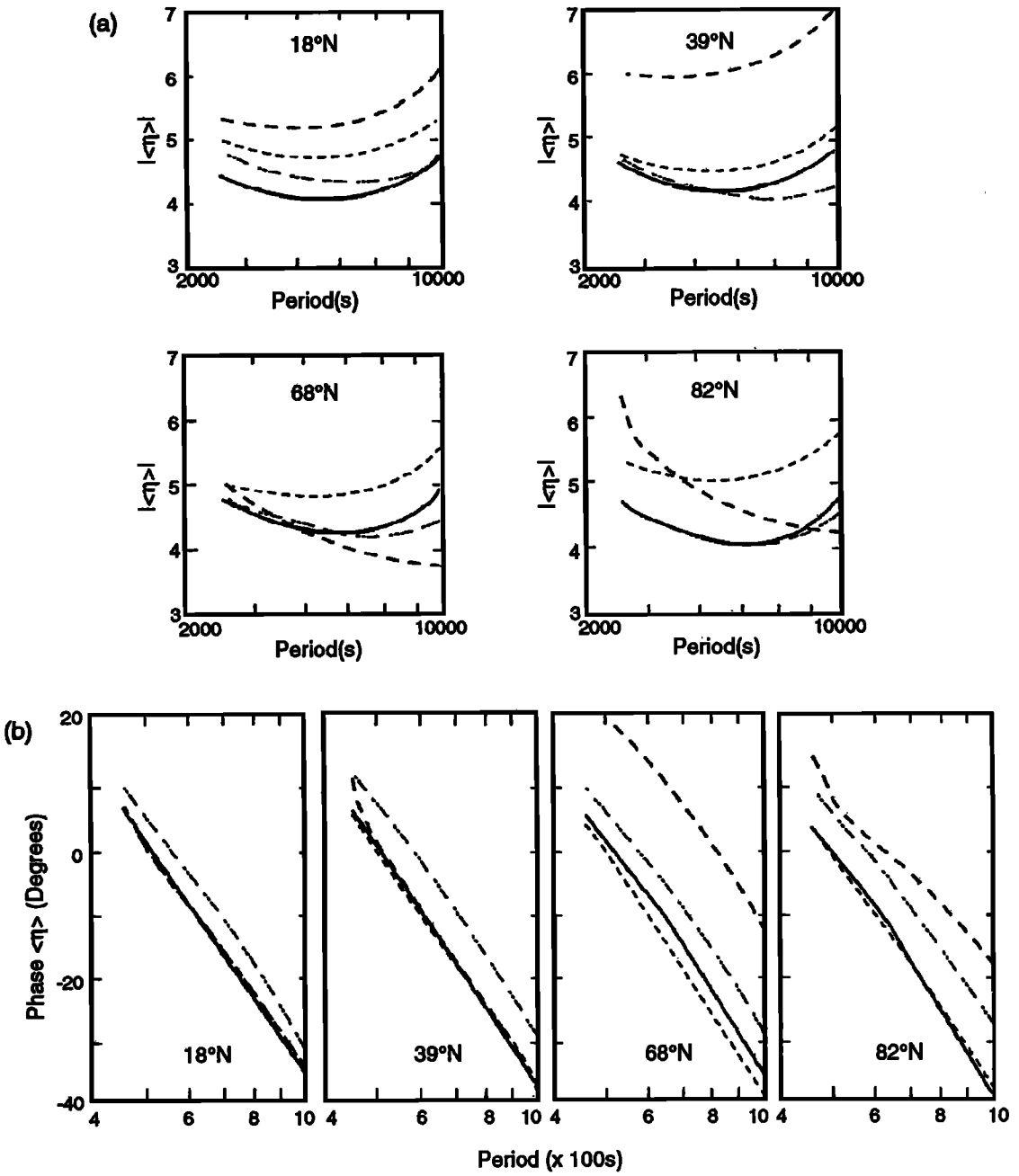

Fig. 10. Similar to Fig. 8 except that λ_x = 1000 km.

Discussion

We did observe in our numerical results some latitudinal trends in both the magnitude and phase of $<\eta>$ for λ_x = 500 km in September, but the trends were limited to a small range of periods. At other times of the year, latitudinal trends in the magnitude or phase of $<\eta>$ are even weaker.

Seasonal trends in the magnitude and phase of $<\eta>$ were found for periods ranging from tens of minutes up to a couple of hours. Seasonal trends in $|<\eta>|$ are clearer than they are in the phase of $<\eta>$. The trends, more noticeable in the shorter wavelength results at all latitudes, could also be seen in the longer wavelength results at low latitudes. Trends were hard to detect in our long-wavelength, high-latitude results.

At intermediate periods (the exact periods depend on λ_x) possible trends in the derived values of $<\eta>$ could be masked by interference effects. These interference effects have been discussed in detail by *Hines and Tarasick* [1987], *Schubert and Walterscheid* [1988] and *Schubert et al.* [1991]. They are important for waves having vertical wavelengths that are less than or comparable to the emission layer thickness, and so are not important for very short period gravity waves having large vertical wavelengths. Although interference effects are important for very long period gravity waves, the vertical wavelength of a gravity wave approaches a constant at long periods in the presence of dissipation (see Figure 5) so that the interference effects do not change as period increases. However, at intermediate periods the effects of interference are important because these waves have vertical wavelengths comparable to the emission layer thickness. Furthermore, at

these periods the vertical wavelength of a gravity wave is still decreasing with increasing period so that the interference effects are also changing with increasing period. It is these rapid changes in interference effects due to changing period that manifest themselves as large oscillations in $<\eta>$ in our computed results at intermediate wave periods.

The larger values of $|<\eta>|$ have generally been associated with smaller ozone densities, although at short wave periods dynamics dominates over chemistry in the determination of $<\eta>$ [*Walterscheid et al.*, 1987]. Examination of our results shows that variations in values of $|<\eta>|$ with season or latitude do not, in general, follow seasonal or latitudinal variations in ozone density around the peak emission altitude. However, the seasonal or latitudinal variations of the undisturbed temperature around the peak emission altitude affect $<\eta>$ because some of the chemical rate constants are temperature dependent. Numerical experimentation has shown that a decrease in the undisturbed temperature will cause a corresponding increase in $|<\eta>|$ at short gravity wave periods.

We therefore compare seasonal variations in background temperatures (Figure 2) with seasonal variations in $|<\eta>|$ (Figures 8-10). We can see that at altitudes around the peak of the OH emission (84-87 km) the June temperatures are consistently smallest, the December temperatures are consistently largest, and the equinox temperatures lie about midway between the two extremes. For most of our results we find that $|<\eta>|$ is consistently largest in June and smallest in December, with the equinox values lying somewhere between the two. Although the differences between temperature extremes become larger at higher latitudes, the corresponding differences in $|<\eta>|$ do not. Also, the high-latitude results for $\lambda_x = 1000$ km do not fit into the simple scenario where short-period values of $<\eta>$ are strongly affected by the background temperature through the temperature dependencies of the rate constants.

We must emphasize that the assumption of an isothermal atmosphere will not be strictly valid at short periods because the variations in temperature over altitude could be large within the large vertical wavelengths of these waves.

CONCLUSIONS

We have used the model described by *Schubert et al.* [1991] to calculate the gravity wave-driven fluctuations in the OH nightglow using output from the model of *Garcia and Solomon* [1985] to define the basic undisturbed state of the nightside mesosphere. In particular, we have examined the seasonal and latitudinal variations in our model-derived values of $<\eta>$ and tried to explain these in terms of seasonal and latitudinal variations in the basic state parameters.

Seasonal or latitudinal variations in our derived values of $<\eta>$ occurred primarily at periods of tens of minutes up to a few hours. Some latitudinal trends were found, but these cases represented only one quarter of all such cases considered. Therefore we conclude that systematic latitudinal trends in $<\eta>$ will be difficult but not impossible to observe.

We had more success in finding significant systematic seasonal variations in our derived values of $<\eta>$. These occurred at periods of tens of minutes up to a couple of hours and appeared more clearly in the magnitude of $<\eta>$ rather than its phase. These short-period results, being most affected by dynamics, were strongly influenced by the seasonal variations in the mesopause temperatures. Based on some numerical experimentation, the seasonal variations in $|<\eta>|$ followed the seasonal variations in mesopause temperature in an expected manner, with the smaller June temperatures (in the northern hemisphere) leading to larger values of $|<\eta>|$ and the larger December temperatures leading to smaller values of $|<\eta>|$. The case of $\lambda_x = 1000$ km at high latitudes was an exception that cannot be simply explained. Therefore we conclude that systematic seasonal trends in $<\eta>$ are likely to be observed at periods of tens of minutes (for waves with $\lambda_x = 100$ km) up to a couple of hours (for waves with $\lambda_x = 1000$ km).

Any seasonal or latitudinal variations that might exist at intermediate periods could be masked by the effects of interference. At long periods, the introduction of the dissipative effects of eddy diffusivity of heat and momentum increases the importance of dynamics so that dynamics and chemistry become of comparable importance. Therefore any seasonal or latitudinal variations in $<\eta>$ that result from seasonal or latitudinal variations in chemistry (minor species number densities and temperature) might be offset by corresponding variations in $<\eta>$ that result from seasonal or latitudinal variations in dynamics (eddy diffusivities). Whether or not the seasonal/latitudinal variations in K_{zz} reinforce or mitigate the seasonal/latitudinal variations in $<\eta>$ (that are themselves due to variations in minor species number densities) is difficult to predict due to the complicated convolution of various parameters that are equally important at long wave periods.

Acknowledgments. This work was supported by NASA under contracts NAS8-36639 and NAS8-38333 (M.P.H.) and the Aerospace Sponsored Research Program (G.S. and R.L.W.). We are indebted to Susan Solomon, Rolando Garcia and Helene Le Texier for supplying tabulations of output from the Garcia-Solomon model.

The editor thanks C.O. Hines and R.M. Johnson for their assistance in evaluating this paper.

REFERENCES

Abreu, V. J., and J. H. Yee, Diurnal and seasonal variation of the nighttime OH (8-3) emission at low latitudes, *J. Geophys. Res.*, *94*, 11,949-11,957, 1989.

Garcia, R. R., and S. Solomon, The effects of breaking gravity waves on the dynamics and chemical composition of the mesosphere and lower thermosphere, *J. Geophys. Res.*, *90*, 3850-3868, 1985.

Hickey, M. P., Effects of eddy viscosity and thermal conduction and coriolis force in the dynamics of gravity wave driven fluctuations in the OH nightglow, *J. Geophys. Res.*, *93*, 4077-4088, 1988a.

Hickey, M. P., Wavelength dependence of eddy dissipation and coriolis force in the dynamics of gravity wave driven fluctuations in the OH nightglow, *J. Geophys. Res.*, *93*, 4089-4101, 1988b.

Hickey, M. P., and K. D. Cole, A quartic dispersion equation for internal gravity waves in the thermosphere, *J. Atmos. Terr. Phys.*, *49*, 889-899, 1987.

Hickey, M. P., and K. D. Cole, A numerical model for gravity wave dissipation in the thermosphere, *J. Atmos. Terr. Phys.*, *50*, 689-697, 1988.

Hines, C. O., and D. W. Tarasick, On the detection and utilization of gravity waves in airglow studies, *Planet. Space Sci.*, *35*, 851-866, 1987.

Hirota, I., Climatology of gravity waves in the middle atmosphere, *J. Atmos. Terr. Phys.*, *46*, 767-773, 1984.

Klostermeyer, J., Influence of viscosity, thermal conduction and ion-drag on the propagation of atmospheric gravity waves in the thermosphere, *Z. Geophys.*, *38*, 881-890, 1972.

Krassovsky, V. I., Infrasonic variations of OH emission in the upper atmosphere, *Ann. Geophys.*, *28*, 739-746, 1972.

Le Texier, H., S. Solomon, and R. R. Garcia, Seasonal variability of the OH Meinel bands, *Planet. Space Sci.*, *35*, 977-989, 1987.

Lindzen, R. S., Turbulence and stress owing to gravity wave and tidal break down, *J. Geophys. Res.*, *86*, 9707-9714, 1981.

Lindzen, R. S. and J. M. Forbes, Turbulence originating from convectively unstable internal gravity waves, *J. Geophys. Res.*, *88*, 6549-6553, 1983.

Pitteway, M. L. V. and C. O. Hines, The viscous damping of atmospheric gravity waves, *Can. J. Phys.*, *41*, 1935-1948, 1963.

Schubert, G., and R. L. Walterscheid, Wave-driven fluctuations in OH nightglow from an extended source region, *J. Geophys. Res.*, *93*, 9903-9915, 1988.

Schubert, G., R. L. Walterscheid, and M. P. Hickey, Gravity wave-driven fluctuations in OH nightglow from an extended, dissipative emission region, *J. Geophys. Res.*, *96*, 13,869-13,880, 1991

Walterscheid, R. L., and G. Schubert, A dynamical-chemical model of tidally driven fluctuations in the OH nightglow, *J. Geophys. Res.*, *92*, 8775-8780, 1987.

Walterscheid, R. L., G. Schubert, and J. Straus, A dynamical-chemical model of wave-driven fluctuations in the OH nightglow, *J. Geophys. Res.*, *92*, 1241- 1254, 1987.

Winick, J. R., Photochemical processes in the mesosphere and lower thermosphere, in *Solar-Terrestrial Physics*, edited by R. L. Carovillano and J. M. Forbes, pp. 677-732, D. Reidel, Hingham, Mass., 1983.

M. P. Hickey, Physitron Inc., 3325 Triana Blvd., Huntsville, AL 35805.

G. Schubert and R. L. Walterscheid, Space Science Laboratory, The Aerospace Corporation, Los Angeles, CA 90009.

(Received January 10, 1992;
revised April 2, 1992;
accepted April 2, 1992.)